Theoretical analysis of structural stability of TM_5Si_3 transition metal silicides

Yue Chen (陈粤),[1,2,*] A. N. Kolmogorov,[2] D. G. Pettifor,[2] Jia-Xiang Shang (尚家香),[1] and Yue Zhang (张跃)[1]
[1]*School of Materials Science and Engineering, Beijing University of Aeronautics and Astronautics, Beijing 100083, China*
[2]*Department of Materials, University of Oxford, Parks Road, Oxford OX1 3PH, United Kingdom*
(Received 20 July 2010; published 9 November 2010)

A combination of electronic-structure calculations from density-functional theory (DFT) through a tight-binding (TB) model to analytic bond-order potentials (BOPs) has been used to investigate the structural trend of the TM_5Si_3 compounds across the early transition metals (TM). First of all, the formation energies of TM_5Si_3, whose ground states adopt the competing $D8_8$, $D8_l$, or $D8_m$ structure types, have been calculated by using DFT (TM is Ti, Zr, Hf, V, Nb, Ta, Cr, Mo, or W). In agreement with experiments the DFT results predict the observed $D8_8 \rightarrow D8_m$ structural trend across the 3*d* series and the $D8_8 \rightarrow D8_l \rightarrow D8_m$ trend across the 4*d* and 5*d* series. A *p-d* canonical TB model is then shown to reproduce these trends, thereby providing a valid basis for the application of BOP theory. By performing a moment analysis within the BOP formalism, we conclude that up to the fifth moment of the density of states is required to explain the structural trend across the 3*d* series whereas up to the ninth moment is required for the 4*d* and 5*d* series.

DOI: 10.1103/PhysRevB.82.184104 PACS number(s): 71.15.Nc, 71.20.Lp

I. INTRODUCTION

Interest in the early transition metal silicides with the 5:3 stoichiometry (TM_5Si_3), which began 60 years ago and continues today, is primarily a result of their high melting points (>2300 K), wide homogeneity ranges and solubility of different alloying elements.[1] There are numerous reports on these materials with regard to their synthesis,[2,3] mechanical properties at room or high temperature,[4,5] oxidation behavior,[6] and thermal expansion anisotropy.[7] Early modeling work on transition metal silicides was carried out with molecular-orbital based methods and focused on the conducting and structural properties of silicide/silicon interfaces: several studies explored the bonding and electronic structure trends in near-noble metal silicides.[8–10] Tight-binding (TB) molecular dynamics simulations proved useful in clarifying the physical picture of structural transformations in Ni, Co, and Fe silicides.[11] Recent theoretical work on selected TM-Si binary systems has been based primarily on density-functional theory (DFT) that provided accurate information about their thermodynamic stability, propensity to form alloys, and a range of electronic, elastic, and thermodynamic properties.[12–17]

In this study we investigate structural trends of the TM_5Si_3 compounds across groups IV to VI of the transition metal series using a combination of theoretical methods. We aim to (i) examine the ability of DFT and a *p-d* canonical TB model to reproduce the observed structural trends of the TM silicides and (ii) establish the relationship between the moments of the electronic density of states (DOS) and the compounds' relative stability in the framework of analytic bond-order potentials (BOPs).[18] It has been shown that BOPs, derived from the first-principles DFT through a series of well-defined approximations yet retaining the linear scaling performance of classical potentials, offer a good balance between accuracy and efficiency;[19,20] it can be used for large-scale simulations of materials mechanical properties, interface geometries, and thin-film growth.[21–23] Our present moments analysis reveals, in particular, what information about the local atomic environment is required in order to provide a reliable description of this class of materials.

The paper is organized as follows: in Sec. II we discuss the topology of the TM_5Si_3 structure types, in Sec. III we describe the methodology, in Secs. IV–VI we present our DFT, tight-binding and BOP results, respectively, and in Sec. VII we conclude.

II. TOPOLOGY OF TM_5Si_3 Structure Types

The structural trends of the TM_5Si_3 compounds across group IV to VI of the transition metal series are clearly observed within the 5:3 Pettifor map in Fig. 9 of Ref. 24. For the TM of group IV (Ti, Zr and Hf), the ground states of the TM_5Si_3 compounds take the $D8_8$ structure. For the TM of group V (Nb and Ta), the ground states take the $D8_l$ structure. Vanadium, on the other hand, displays $D8_m$ as the ground state structure, as also do Cr, Mo, and W in group VI. Thus, we have the $D8_8 \rightarrow D8_m$ and $D8_8 \rightarrow D8_l \rightarrow D8_m$ structural trends as we go across the early 3*d* and 4*d*/5*d* TM elements, respectively.

The coordination polyhedra of the $D8_8$, $D8_l$, and $D8_m$ crystal structures are shown in Fig. 1. All three structures have 16 atoms in their primitive cells but the number of nonequivalent sites is different. In the $D8_8$, there are three nonequivalent sites which are denoted by TM1, TM2, and Si. In the $D8_l$ and $D8_m$, there are four nonequivalent sites denoted by TM1, TM2, Si1, and Si2. The percentage of each nonequivalent site is also given in this figure. The assignation of atoms to the local coordination polyhedra is determined by using the maximum gap rule as illustrated in Fig. 2 which gives nearest-neighbor information about each nonequivalent site. We see that the TM1 sites in all the structures have a CN of 14 but the coordination polyhedra differ in composition (namely, 4Si+10TM in $D8_m$; 6Si+8TM in $D8_8$ and $D8_l$) and distribution of neighbors in the first shell (namely, 4Si in $D8_l$; 2TM in $D8_m$ and $D8_8$). The TM2 sites have different CNs (namely, 16 in $D8_l$; 15 in $D8_m$ and $D8_8$) and a more dispersed distribution of the NNs. The distinctive

 ©2010 The American Physical Society

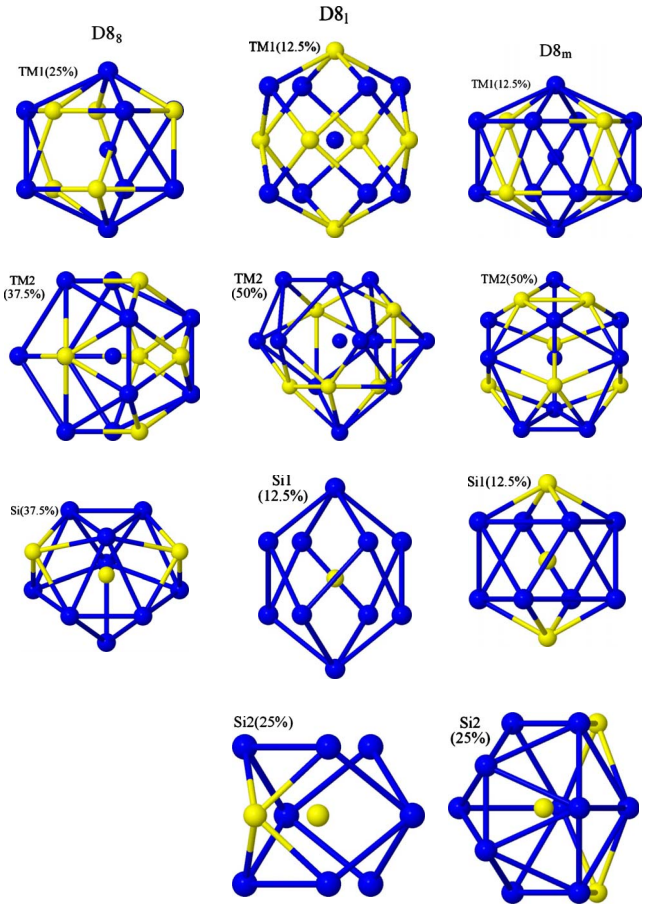

FIG. 1. (Color online) The first, second, and third columns correspond to the coordination polyhedra of the nonequivalent sites in D8$_8$, D8$_l$, and D8$_m$ structures, respectively. The black and white spheres (or blue and yellow in online version) represent the TM and Si atoms, respectively.

feature of the Si1 site in D8$_m$ and the Si2 site in D8$_l$ is the closeness of the first Si NNs resulting from strong *p-p* bonding contributions.

III. METHODOLOGY

The work presented in this paper is done by using a hierarchy of electronic structure methods from first-principles DFT through a physically more intuitive *p-d* canonical TB model to analytic BOP theory. The DFT calculations are carried out with the Vienna *ab initio* simulation package (VASP) (Refs. 25 and 26) within the generalized gradient approximation[27] using projector augmented wave pseudopotentials.[28] An energy cutoff of 480 eV is applied to all of the TM-Si binary systems. A **k**-point mesh of 12 $\times 12 \times 5$ is generated by the Monkhorst-Pack scheme[29] for numerical integrations over the Brillouin zone for the C11$_b$ six-atom unit cell. The same **k**-point density is applied to the other structures. All the systems are fully relaxed, which includes the cell shapes and the internal atomic coordinates, before the calculation of the ground-state energies.

The TB and analytic BOP calculations were carried out by using the Bond-Order Potential from Oxford (BOPfox) package.[30] In both the TB and BOP formalisms, the average binding energy per atom of a system can be expressed as the sum of the repulsive energy and bond energy[31]

$$E = E_{rep} + E_{bond}. \tag{1}$$

It has been shown that the repulsive energy is well described by an empirical pair potential whereas the bond energy arises from the quantum mechanical bonding between neighboring atoms.[21,32–36] The average bond energy per atom takes the following form within the orthogonal TB approximation:[31]

$$E_{bond} = \aleph^{-1} \sum_i \int^{\varepsilon_F} (\varepsilon - \varepsilon_i) n_i(\varepsilon) d\varepsilon, \tag{2}$$

where $\aleph$ is the number of atoms in the unit cell, ε_i is the on-site energy, $n_i(\varepsilon)$ is the local DOS at atom i and ε_F is the Fermi energy. By expanding the local DOS in terms of Chebyshev polynomials of the second kind, the bond energy can be further expressed within analytic BOP theory[18]

$$E_{bond}^{n_{max}} = \frac{b_\infty}{\aleph} \sum_i \sum_{m=0}^{n_{max}} \sigma_i^{(m)} [\hat{\chi}_{m+2}(\phi_F) - \gamma_{i0} \hat{\chi}_{m+1}(\phi_F) + \hat{\chi}_m(\phi_F)], \tag{3}$$

where $\sigma_i^{(m)}$ is an expansion coefficient corresponding to each atomic site i, n_{max} is the level of moment approximation, and γ_{i0} is given by $\gamma_{i0} = (\varepsilon_i - a_\infty)/b_\infty$. a_∞ and b_∞ correspond to the center and one quarter the width of the valence band, respectively. For $m \geq 2$ the reduced response functions in Eq. (3) take the form[37]

$$\hat{\chi}_m(\phi_F) = \frac{1}{\pi} \left\{ \frac{sin[(m+1)\phi_F]}{m+1} - \frac{sin[(m-1)\phi_F]}{m-1} \right\}, \tag{4}$$

where $\phi_F = cos^{-1}[(\varepsilon_F - a_\infty)/2b_\infty]$.

IV. DENSITY-FUNCTIONAL THEORY

We observe from the early TM-Si phase diagrams that 3:1, 2:1, 5:3, 1:1, and 1:2 are the main stoichiometries that the binary intermetallics adopt. A complete set of DFT formation energy calculations of these phases has been carried out for the TMs: Ti, Zr, Hf, V, Nb, Ta, Cr, Mo, and W. The formation energy per atom is given by

$$\Delta E_f = (E_{tot}^{TM_mSi_n} - mE_{tot}^{TM} - nE_{tot}^{Si})/(m+n), \tag{5}$$

where $E_{tot}^{TM_mSi_n}$, E_{tot}^{TM}, and E_{tot}^{Si} are the total energies of the ground-state structures of a TM$_m$Si$_n$ unit cell, a transition metal atom and a silicon atom, respectively. By referring to the Inorganic Crystal Structure Database provided by the Chemical Database Service at Daresbury,[38] we have included the twelve most common structure types of these binary systems in our DFT calculations. They are the A15 and tP32-Ti$_3$P for the 3:1 stoichiometry; the C16 for the 2:1 stoichiometry; the D8$_8$, D8$_l$, and D8$_m$ for the 5:3 stoichiometry; the B20 and B27 for the 1:1 stoichiometry; the C11$_b$, C40, C54, and C49 for the 1:2 stoichiometry. For completeness, the formation energies of the Nb-Si and Mo-Si systems, which we have discussed in our previous publication,[39] are also included in Fig. 3.

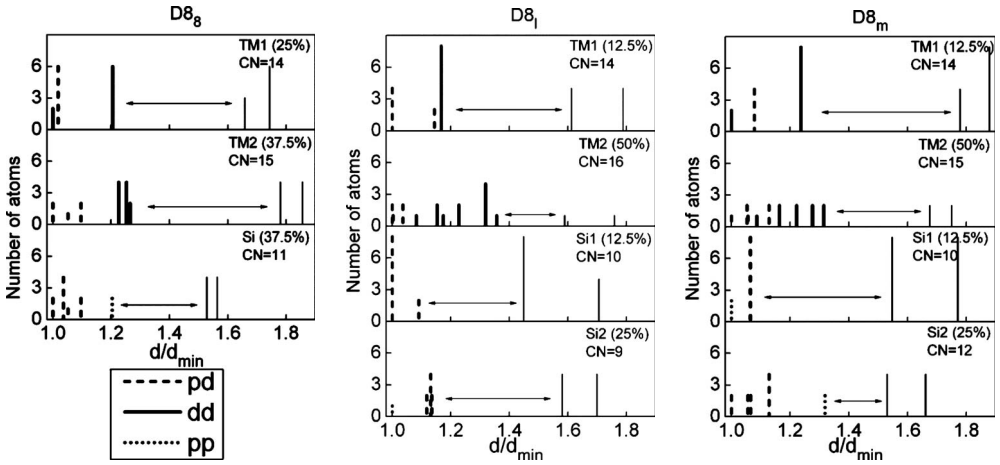

FIG. 2. Nearest-neighbor histograms about the nonequivalent sites in the $D8_8$, $D8_l$, and $D8_m$ structures, showing the number of atoms in a given neighboring shell versus the normalized shell distance (d_{min} is the nearest-neighbor distance). The maximum gap is denoted by a two-sided arrow. The pd, dd and pp histograms denote Si-TM, TM-TM, and Si-Si neighbors, respectively.

The lowest energy structures of the 5:3 and 1:2 stoichiometries which are predicted by DFT (Fig. 3), are tabulated in Table I. It can be seen from both Table I and Fig. 4 that, for the early 4*d* and 5*d* transition metals, our DFT calculations successfully reproduce the experimentally observed $D8_8 \rightarrow D8_l \rightarrow D8_m$ structural trend of the 5:3 stoichiometry as the number of valence *d* electrons increases in moving from IVB through VB to VIB across the periodic table. For the early 3*d* transition metals, we find the stable structures go from the $D8_8$ directly to $D8_m$ with $D8_l$ being omitted ($D8_8 \rightarrow D8_m$).

A discussion on the structural trend within the $TMSi_2$ intermetallics has been given elsewhere.[40] It was found that the structural trend is driven primarily by the $pd\pi$ bond between the nearest-neighbor TM and Si atoms, reflecting the sensitivity of the π bond order to dihedral angles.

Most of the DFT ground-state structures at 0 K are in agreement with experiments but there are a few exceptions. For the 1:2 stoichiometry, the experimentally observed crystal structures of $TiSi_2$ and $CrSi_2$ are C54 and C40, respectively. These structures are stabilized by the entropic contributions at elevated temperatures as discussed by Pankhurst *et al.*[40] and Colinet *et al.*[41] Entropic contributions are most probably also important for CrSi, Cr_5Si_3, and W_5Si_3 since these experimentally observed phases are predicted by DFT to be metastable as their formation energies lie above the tie lines in Fig. 3. As our previous publication[39] has already demonstrated the importance of entropy for Nb-Si and Mo-Si systems, a further study on the entropic contributions is needed to clarify the above ambiguities, and to understand the discrepancies between the experimental observations and theoretical predictions.

Despite the importance of entropy in some particular cases, the emphasis of our current paper is on the phase stabilities at 0 K which arise from the electronic structures, so that the entropic contributions are neglected. In the following sections, we apply the canonical TB model and analytic BOP theory to investigate the origin of the difference of the $D8_8 \rightarrow D8_m$ and $D8_8 \rightarrow D8_l \rightarrow D8_m$ structural trends across the TM_5Si_3 intermetallics.

V. CANONICAL TIGHT-BINDING MODEL

The structural energy difference theorem[42] enables us to compare the stability of two structures by only comparing their bond energies. Starting from Eq. (1), it can be proved that the binding energy difference of any two equilibrium structures can be expressed to first order as

$$\Delta E = (\Delta E_{bond})_{\Delta E_{rep}=0} \tag{6}$$

which implies that only the bond energy needs to be computed if the unit-cell volumes are adjusted to ensure the same repulsive energies. Making the realistic assumption that the pairwise repulsive potential falls off with distance as the square of the bond integrals $\beta(R)$, the constraint $\Delta E_{rep}=0$ is equivalent to $\Delta\Sigma_{i\neq j}[\beta(R_{ij})]^2=0$. On the other hand Cyrot-Lackmann has shown that within TB the *p*th moment of the local DOS on atom i_1 can be written as[43,44]

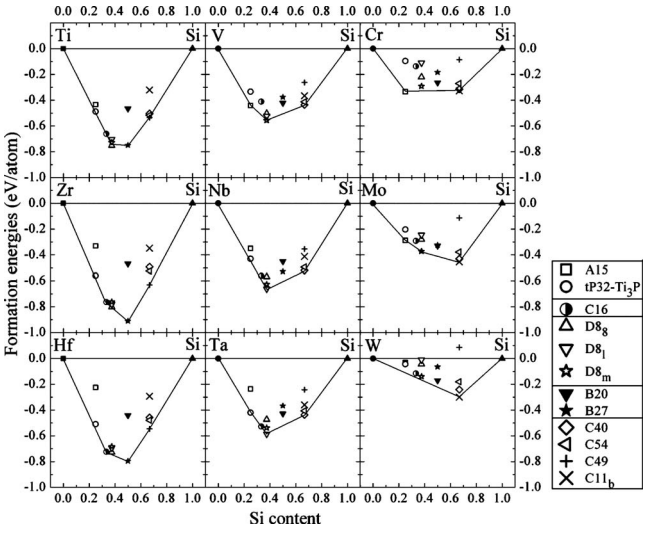

FIG. 3. DFT formation energies of different phases of group IV to VI TM-Si binary systems.

TABLE I. DFT predicted ground-state structures of TM_5Si_3 and $TMSi_2$.

	TM_5Si_3	$TMSi_2$		TM_5Si_3	$TMSi_2$		TM_5Si_3	$TMSi_2$
Ti	$D8_8$	C49	V	$D8_m$	C40	Cr	$D8_m$	$C11_b$
Zr	$D8_8$	C49	Nb	$D8_l$	C40	Mo	$D8_m$	$C11_b$
Hf	$D8_8$	C49	Ta	$D8_l$	C40	W	$D8_m$	$C11_b$

$$\mu_{pi_1} = \sum_{i_2 \ldots i_p} H_{i_1 i_2} H_{i_2 i_3}, \ldots, H_{i_p i_1}. \tag{7}$$

This implies that the pth moment of the local DOS on atom i_1 is the sum over all the hopping (or bonding) paths of length p, that start and finish on atom i_1 within the crystal. Using this link between the second moment μ_{2i} of the local DOS and all self-returning hopping paths of length two, the constraint $\Delta\Sigma_{i\neq j}[\beta(R_{ij})]^2=0$ can be rewritten as $\Delta\mu_2=0$, where μ_2 is the average second moment per atom, namely, $\mu_2=\Sigma_i\mu_{2i}/\aleph$ for $\aleph$ atoms in the unit cell.

In this study, we have taken the pd TB model from Ref. 45 that characterizes the TM and Si atoms by the number of d electrons N_d and p electrons N_p, respectively. The valence s orbitals have been neglected. We have set the difference in the on-site energies $\varepsilon_d-\varepsilon_p=0$, as Pankhurst *et al.* had found that $\varepsilon_d-\varepsilon_p=0$ gave the same structural trends as the DFT value of $\varepsilon_d-\varepsilon_p=-2.24$ eV for $C11_b$ $MoSi_2$ (see Fig. 4 of Ref. 40). Thus, Eq. (6) can be rewritten as

$$\Delta E = (\Delta E_{bond})_{\Delta\mu_2=0} = (\Delta E_{band})_{\Delta\mu_2=0}, \tag{8}$$

where the band energy is defined as[31]

$$E_{band} = \aleph^{-1}\sum_i \int^{\varepsilon_F} \varepsilon n_i(\varepsilon) d\varepsilon. \tag{9}$$

The band energy is equivalent to the bond energy in this TB model since we have taken ε_p and ε_d as the reference energy, namely, $\varepsilon_p=\varepsilon_d=0$. We are now able to compare the stability of two structures by computing only the band energies under the constraint that the second moments of the DOS for the two competing structures are identical.

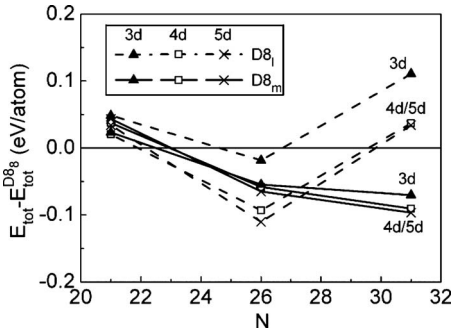

FIG. 4. DFT structural energy differences of $D8_l$ and $D8_m$ with respect to $D8_8$ as a function of the number of Si p and TM d electrons per TM_5Si_3 formula unit, namely, $N=3N_p+5N_d$. For the above DFT plot we have assumed $N_p=2$ and $N_d=N^{TM}-1$, where N^{TM} is the group number of the TM element.

The distance dependences of the bond integrals between the p and d orbitals is described as follows within the canonical TB model:[46]

$$dd(\sigma,\pi,\delta) = (-6,4,-1)(r_d/R)^5,$$

$$pp(\sigma,\pi) = (2,-1)(r_p/R)^3,$$

$$pd(\sigma,\pi) = (-3,3^{1/2})(r_p^3 r_d^5)^{1/2}/R^4, \tag{10}$$

where r_p and r_d are constants that determine the amplitude of the bond integrals. We have taken $r_p=5$ a.u. for Si, and $r_d=3.8$ a.u. for the $3d$ elements and $r_d=4.2$ a.u. for the $4d$ and $5d$ elements, where with R in atomic units the bond integrals in Eq. (10) are given in electron volt. The ratio of the dd bond integrals for the $3d$ transition elements compared to those for the $4d$ and $5d$ elements will, therefore, be given by $(3.8/4.2)^5=0.61$. This is consistent with the $3d$ band widths being approximately 60% those of the corresponding $4d$ and $5d$ elements.

The band energies of the competing structures $D8_8$, $D8_l$, and $D8_m$ have been calculated as a function of the electron count, as plotted in Fig. 5. The validity of this TB model is verified by being able to reproduce the $D8_8 \rightarrow D8_l \rightarrow D8_m$ structural trend for the $4d$ and $5d$ TMs as the electron count increases (right-hand panel in Fig. 5). In addition, the $D8_8 \rightarrow D8_m$ structural trend for the $3d$ TMs is also reproduced (left hand panel in Fig. 5). Despite the approximations which have been made in this simple TB model, the comparison between these TB results in Fig. 5 and the DFT results in Fig. 4 for $20 \leq N \leq 32$ is qualitatively reasonable. In the next section we use analytic BOP theory to expand the bond energy in terms of response functions and expansion coefficients, thereby enabling us to analyze the contributions from the different moments.

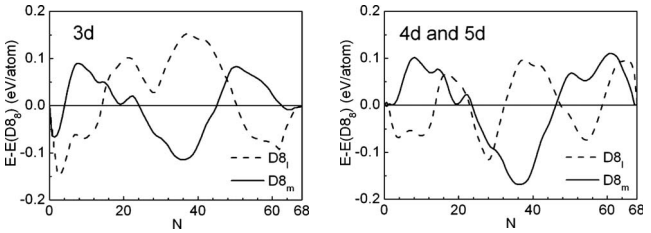

FIG. 5. The band energy difference of the 5:3 stoichiometric compounds calculated with the canonical TB model. The left- and right-hand panels correspond to the $3d$ and $4d/5d$ TMs, respectively. N is the number of valence electrons per formula unit.

VI. BOND-ORDER POTENTIALS

Turchi and Ducastelle[47] have shown that the difference in the band energy between two structures can be expressed to first order in $\Delta\varepsilon_F$ as

$$\Delta E_{band} = \int^{\varepsilon_F} (\varepsilon - \varepsilon_F)\Delta n(\varepsilon) d\varepsilon, \tag{11}$$

where $n(\varepsilon) = \aleph^{-1}\Sigma_i n_i(\varepsilon)$. It follows from Eq. (3) above and Eq. 46 in Ref. 18 that within analytic BOP theory this can be written as

$$\Delta E_{band}^{n_{max}} = b_\infty \sum_{m=3}^{n_{max}} \Delta\sigma^{(m)}[\hat{\chi}_{m+2}(\phi_F) - 2\ cos\ \phi_F \hat{\chi}_{m+1}(\phi_F) + \hat{\chi}_m(\phi_F)], \tag{12}$$

where n_{max} is the largest exact moment retained within the above series expansion. $\sigma^{(m)}$ gives the sum over all atoms in the unit cell of the local expansion coefficients $\sigma_i^{(m)}$ normalized by the number of atoms $\aleph$. These coefficients depend on the environment through the moments as in Eq. 36 of Ref. 18. We have assumed that a_∞ and b_∞ in Eq. (12) are structure independent and given by the center and one quarter the width, respectively, of the $D8_m$ TB valence band, namely, $a_\infty = -1.20$ eV, $b_\infty = 2.93$ eV for the $3d$ TMs and $a_\infty = -0.53$ eV, $b_\infty = 3.82$ eV for the $4d/5d$ TMs. The above series for the *difference* in the band energy does not include the second moment contributions because they vanish through the structural energy difference theorem with $\Delta\mu_2 = 0$.

Substituting the response functions from Eq. (4) into Eq. (12) leads after several steps of trigonometry to the reduced form[48]

$$\Delta E_{band}^{n_{max}} = b_\infty \sum_{m=3}^{n_{max}} \hat{\hat{\chi}}_m(\phi_F)\Delta\sigma^{(m)}, \tag{13}$$

where

$$\hat{\hat{\chi}}_m(\phi_F) = \frac{1}{\pi}\left\{\frac{2\ sin[(m+1)\phi_F]}{m(m+2)} - \frac{sin[(m+3)\phi_F]}{(m+2)(m+3)} - \frac{sin[(m-1)\phi_F]}{m(m-1)}\right\}. \tag{14}$$

These reduced response functions were first derived by Turchi and Ducastelle.[47] However, whereas their theory used the linear Green's function method, $\Delta\sigma^{(m)}$ in Eq. (13) includes nonlinear contributions as well (see Table II of Ref. 18). Thus, the energy difference between two structure-types may be expressed as a sum over the different moment contributions. The mth contribution factorizes as the product of a canonical response function $\hat{\hat{\chi}}_m$ that has $(m-2)$ nodes as a function of band filling (see Fig. 1 of Ref. 47) and the difference $\Delta\sigma^{(m)}$ that depends explicitly on all the local moments up to the mth (see Eq. 36 of Ref. 18).

Figures 6 and 7 show the convergence of the energy differences as a function of the maximum number of moments n_{max} for the $3d$ and $4d/5d$ TM_5Si_3 systems, respectively. We see from Fig. 6 that for the $3d$ case the curves agree qualitatively with the TB results in the left-hand panel of Fig. 5 by

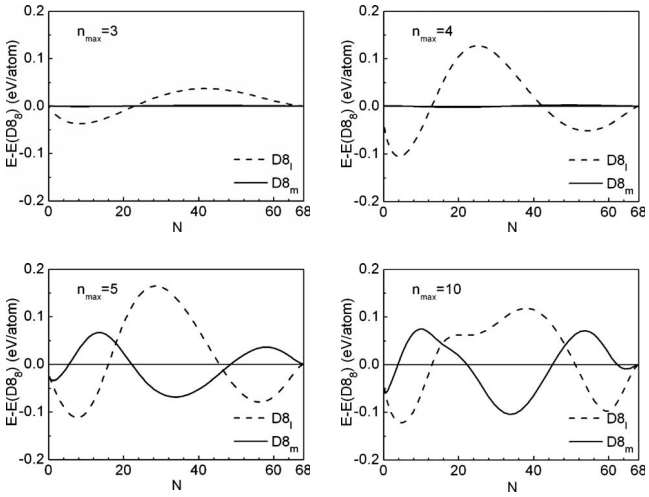

FIG. 6. Convergence of the structural energy differences as a function of the maximum number of moments for the $D8_m$-$D8_8$ (solid curve) and $D8_l$-$D8_8$ (dashed curve) $3d$ TM_5Si_3 systems.

$n_{max} = 5$. Interestingly there is no visible distinction energetically between $D8_m$ and $D8_8$ up to $n_{max} = 4$. This is due to their values of $\sigma^{(3)}$ and $\sigma^{(4)}$ being almost identical, even though the *individual* site contributions $\sigma_i^{(3)}$ and $\sigma_i^{(4)}$ differ markedly as expected from Figs. 1 and 2. By the time we reach $n_{max} = 10$ the relative positions of the nodes are in excellent agreement with the TB results. On the other hand, however, we see from Fig. 7 that for the $4d/5d$ case the oscillatory structure of the $(D8_l$-$D8_m)$ curve is only reproduced by $n_{max} = 9$. Again excellent agreement with the TB results in the right-hand panel of Fig. 5 is given by $n_{max} = 10$.

This dependence of the structural trends on high-moment contributions is reminiscent of the case for the fcc versus hcp stability of elemental transition metals where up to the sixth moment is required.[49,50] Unlike the bcc versus fcc case where the four-atom ring contributions to the fourth moment drive the bcc stability in groups V and VI,[50,51] no one par-

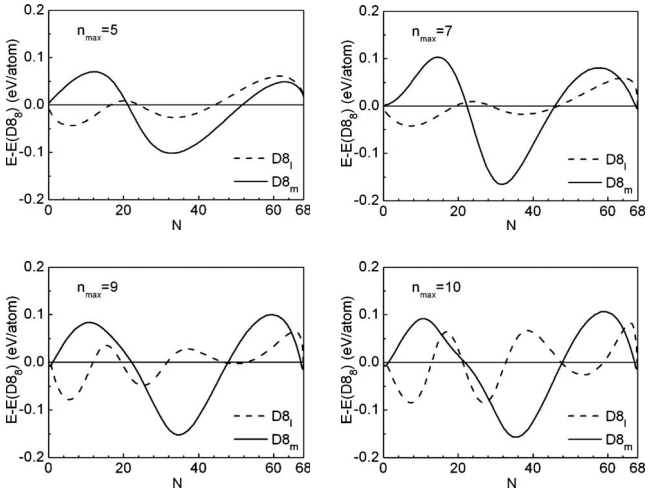

FIG. 7. Convergence of the structural energy differences as a function of the maximum number of moments for the $D8_m$-$D8_8$ (solid curve) and $D8_l$-$D8_8$ (dashed curve) $4d/5d$ TM_5Si_3 systems.

ticular moment path can be identified for the fcc-hcp structural trend.[49] It is, therefore, perhaps not surprising that the much more complicated situation of the TM_5Si_3 structure-types with their multiple nonequivalent sites also allows no simple moment path to be identified as driving the observed structural trends.

VII. CONCLUSIONS

We have investigated the structural trend of the TM_5Si_3 compounds across the early transition metals by performing a hierarchy of electronic structure calculations from first-principles DFT through the more physically intuitive TB model to analytic BOP theory. The DFT heats of formation were in agreement with the experimentally observed $D8_8 \rightarrow D8_m$ structural trend across the 3*d* series and the $D8_8 \rightarrow D8_l \rightarrow D8_m$ trend across the 4*d* and 5*d* series. The application of a simple *p-d* canonical TB model together with the structural energy difference theorem was shown to reproduce these structural trends. Analytic BOP theory using these TB parameters as input then demonstrated that the $D8_8 \rightarrow D8_m$ structural trend across the 3*d* series required up to the fifth moment of the density of states whereas the $D8_8 \rightarrow D8_l \rightarrow D8_m$ trend across the 4*d* and 5*d* series required up to the ninth moment. Similar to the well-studied case of the fcc versus hcp stability across the elemental transition metal series, no single moment path can be identified as driving the structural trends across the TM_5Si_3 series.

ACKNOWLEDGMENTS

We would like to thank Bernhard Seiser for advice on the BOPfox package, the National Nature Science Foundation of China (Grant No. 50771004) for financial support. Y.C. is grateful to the China Scholarship Council for financial support and the Department of Materials, University of Oxford for their hospitality and use of computing facilities in the Materials Modeling Laboratory.

*Corresponding author; yuechen@imr.ac.cn

[1] J. J. Williams, Y. Y. Ye, M. J. Kramer, K. M. Ho, L. Hong, C. L. Fu, and S. K. Malik, Intermetallics **8**, 937 (2000).
[2] P. B. Celis and K. Ishizaki, J. Mater. Sci. **26**, 3497 (1991).
[3] C. L. Yeh and W. H. Chen, J. Alloys Compd. **439**, 59 (2007).
[4] L. Zhang and J. Wu, Acta Mater. **46**, 3535 (1998).
[5] Y. X. Yin and H. M. Wang, Mater. Sci. Eng., A **452-453**, 746 (2007).
[6] J. Williams and M. Akinc, Intermetallics **6**, 269 (1998).
[7] J. H. Schneibel, C. J. Rawn, T. R. Watkins, and E. A. Payzant, Phys. Rev. B **65**, 134112 (2002).
[8] P. S. Ho, G. W. Rubloff, J. E. Lewis, V. L. Moruzzi, and A. R. Williams, Phys. Rev. B **22**, 4784 (1980).
[9] R. M. Boulet, A. E. Dunsworth, J. P. Jan, and H. L. Skriver, J. Phys. F: Met. Phys. **10**, 2197 (1980).
[10] O. Bisi and C. Calandra, J. Phys. C **14**, 5479 (1981).
[11] L. Miglio, F. Tavazza, A. Garbelli, and M. Celino, *Tight-Binding Approach to Computational Materials Science*, MRS Symposium Proceedings No. 491 (Materials Research Society, Pittsburgh, 1998), p. 309, and references therein.
[12] Y. Chen, J. X. Shang, and Y. Zhang, J. Phys.: Condens. Matter **19**, 016215 (2007).
[13] Y. Chen, J. X. Shang, and Y. Zhang, Phys. Rev. B **76**, 184204 (2007).
[14] X. M. Tao, P. Jund, C. Colinet, and J. C. Tedenac, Phys. Rev. B **80**, 104103 (2009).
[15] M. Ekman and V. Ozolins, Phys. Rev. B **57**, 4419 (1998).
[16] S. Brutti, D. Nguyen-Manh, D. G. Pettifor, P. Manfrinetti, M. Napoletano, and F. Canepa, Calphad **33**, 260 (2009).
[17] X. M. Tao, P. Jund, C. Colinet, and J. C. Tedenac, Intermetallics **18**, 688 (2010).
[18] R. Drautz and D. G. Pettifor, Phys. Rev. B **74**, 174117 (2006).
[19] R. Drautz, X. W. Zhou, D. A. Murdick, B. Gillespie, H. N. G. Wadley, and D. G. Pettifor, Prog. Mater. Sci. **52**, 196 (2007).
[20] M. Aoki, D. Nguyen-Manh, D. G. Pettifor, and V. Vitek, Prog. Mater. Sci. **52**, 154 (2007).
[21] M. Mrovec, R. Groger, A. G. Bailey, D. Nguyen-Manh, C. Elsasser, and V. Vitek, Phys. Rev. B **75**, 104119 (2007).
[22] D. A. Murdick, X. W. Zhou, H. N. G. Wadley, D. Nguyen-Manh, R. Drautz, and D. G. Pettifor, Phys. Rev. B **73**, 045206 (2006).
[23] M. Mrovec, M. Moseler, C. Elsasser, and P. Gumbsch, Prog. Mater. Sci. **52**, 230 (2007).
[24] D. G. Pettifor, J. Phys. C **19**, 285 (1986).
[25] G. Kresse and J. Hafner, Phys. Rev. B **47**, 558 (1993).
[26] G. Kresse and J. Hafner, Phys. Rev. B **49**, 14251 (1994).
[27] J. P. Perdew and Y. Wang, Phys. Rev. B **45**, 13244 (1992).
[28] P. E. Blöchl, Phys. Rev. B **50**, 17953 (1994).
[29] H. J. Monkhorst and J. D. Pack, Phys. Rev. B **13**, 5188 (1976).
[30] T. Hammerschmidt, B. Seiser, M. Ford, D. G. Pettifor, and R. Drautz, BOPfox program for tight-binding and bond-order potential calculations (unpublished).
[31] M. Finnis, *Interatomic Forces in Condensed Matter* (Oxford University Press, New York, 2003).
[32] R. Drautz, D. A. Murdick, D. Nguyen-Manh, X. W. Zhou, H. N. G. Wadley, and D. G. Pettifor, Phys. Rev. B **72**, 144105 (2005).
[33] M. J. Cawkwell, M. Mrovec, D. Nguyen-Manh, D. G. Pettifor, and V. Vitek, *A Bond-Order Potential Incorporating Analytic Screening Functions for the Molybdenum Silicides*, MRS Symposium Proceedings, No. 842 (Materials Research Society, Warrendale, 2005), Paper S2.8.
[34] K. E. Tan, A. M. Bratkovsky, R. M. Harris, A. P. Horsfield, D. Nguyen-Manh, D. G. Pettifor, and A. P. Sutton, Modell. Simul. Mater. Sci. Eng. **5**, 187 (1997).
[35] M. Mrovec, D. Nguyen-Manh, D. G. Pettifor, and V. Vitek, Phys. Rev. B **69**, 094115 (2004).
[36] S. Znam, D. Nguyen-Manh, D. G. Pettifor, and V. Vitek, Philos. Mag. **83**, 415 (2003).
[37] D. G. Pettifor, Phys. Rev. Lett. **63**, 2480 (1989).
[38] D. A. Fletcher, R. F. McMeeking, and D. Parkin, J. Chem. Inf. Comput. Sci. **36**, 746 (1996).
[39] Y. Chen, T. Hammerschmidt, D. G. Pettifor, J. X. Shang, and Y. Zhang, Acta Mater. **57**, 2657 (2009).

[40] D. A. Pankhurst, D. Nguyen-Manh, and D. G. Pettifor, Phys. Rev. B **69**, 075113 (2004).
[41] C. Colinet, W. Wolf, R. Podloucky, and A. Pasturel, Appl. Phys. Lett. **87**, 041910 (2005).
[42] D. G. Pettifor, *Bonding and Structure of Molecules and Solids* (Oxford University Press, New York, 1995).
[43] F. Ducastelle and F. Cyrot-Lackmann, J. Phys. Chem. Solids **32**, 285 (1971).
[44] F. Cyrot-Lackmann, Adv. Phys. **16**, 393 (1967).
[45] D. G. Pettifor and R. Podloucky, J. Phys. C **19**, 315 (1986).
[46] O. K. Andersen, W. Klose, and H. Nohl, Phys. Rev. B **17**, 1209 (1978).
[47] P. Turchi and F. Ducastelle, in *The Recursion Method and its Applications*, Springer Series in Solid-State Sciences Vol. 58, edited by D. G. Pettifor and D. L. Weaire (Springer, London, 1985), p. 104.
[48] B. Seiser, R. Drautz, and D. G. Pettifor (private communication).
[49] P. Turchi, Ph.D. thesis, University of Paris VI, 1984.
[50] D. G. Pettifor and M. Aoki, Philos. Trans. R. Soc. London, Ser. A **334**, 439 (1991).
[51] J. A. Moriarty, Phys. Rev. B **42**, 1609 (1990).